

# Radii of proton emitters

Y. R. Lin (林雅茹)<sup>1,2</sup> S. M. Wang (王思敏)<sup>1,2,\*</sup> and W. Nazarewicz<sup>3,4,†</sup>

<sup>1</sup>Key Laboratory of Nuclear Physics and Ion-beam Application (MOE),  
Institute of Modern Physics, Fudan University, Shanghai 200433, China

<sup>2</sup>Shanghai Research Center for Theoretical Nuclear Physics,  
NSFC and Fudan University, Shanghai 200438, China

<sup>3</sup>Facility for Rare Isotope Beams, Michigan State University, East Lansing, Michigan 48824, USA

<sup>4</sup>Department of Physics and Astronomy, Michigan State University, East Lansing, Michigan 48824, USA

(Dated: November 14, 2025)

Nuclear radius is a fundamental structural observable that informs many properties of atomic nuclei and nuclear matter. Experimental studies of radii in dripline nuclei are in the forefront of research with radioactive ion beams. Of particular interest are charge radii of proton-unbound nuclei that will soon be approached in laser spectroscopy. In this paper, using the complex-energy approach and direct time propagation, we investigate the radius of the proton resonance whose size is ill-defined in the standard stationary quantum-mechanical description. An early-time plateau is identified during which the radius of the Gamow resonance coincides with the real-energy radius accessible experimentally. We demonstrate a non-monotonic dependence of the complex radius on decay energy and a local increase of the charge radius across the threshold (a proton halo effect).

*Introduction.* — The limits of nuclear landscape are formally marked by particle drip lines, beyond which the nucleonic decays are possible because of positive decay  $Q$ -values. Moving away from drip lines by adding protons or neutrons, one encounters a zone of metastable states (long-lived resonances) that are amenable to experimental investigations. This zone is fairly extended on the proton-rich side because of the presence of the Coulomb barrier. Further away from the drip lines, one enters the ephemeral zone of very short-lived nuclear states where the very notion of nuclear existence may become questionable [1, 2].

Proton emitters are narrow resonances beyond the proton drip line [3–8]. Since their lifetimes primarily depend on  $Q$ -values and angular momentum, studies of proton emitters provide unique information on nuclear structure and reactions in the presence of the low-lying proton continuum. Energetically, proton-emitting nuclei are clustered in a rather narrow window of  $Q$ -values [9, 10]. For the large  $Q_{1p/2p}$ -values, decay lifetimes are going to be too fast to be observed ( $T_{1p/2p} < 100$  ns). On the other hand, if  $Q_{1p/2p}$ -values are too low ( $T_{1p/2p} > 100$  ms), proton-decay rates cannot compete with other decay modes, such as  $\beta^+$ , EC, or  $\alpha$  decays.

Matter radii of unstable nuclei can be studied using hadronic probes by measuring reaction and interaction cross sections [11, 12]. The proton and neutron radii extracted in this way, are prone to appreciable uncertainties because of reaction modeling. The precise information on sizes of unstable nuclei comes, therefore, from studies of nuclear charge radii. Indeed, due to experimental progress in laser spectroscopy, nuclear charge radii can now be measured along long isotopic chains of short-lived

isotopes [13, 14]. The future experimental programs in this area intend to investigate charge radii of nuclei close to and beyond the proton drip line [15, 16]. This exciting perspective raises several theoretical challenges.

For nuclei that are formally bound, but close to dripline, low-energy scattering continuum can impact nuclear radii. Here, excellent examples are nuclear halos [17] and radial properties of proton-rich nuclei such as  $^{36}\text{Ca}$  [18–20]. For unbound nuclear states, the notion of the root-mean-square (rms) radius becomes problematic as resonances are not stationary. For extremely narrow states, it is customary to use the bound-state approximation, in which the scattering tail of the wave function is neglected. For states with shorter lifetimes, however, the real-energy stationary approach cannot be used as the scattering tail of the one-body density would formally result in an infinite rms radius. The two alternative methods are: (i) the time-dependent formalism based on the explicit solution of the time-dependent Schrödinger equation (TDSE) or (ii) stationary complex-energy resonant-state approach in which the outgoing boundary condition is imposed. While the former method is not effective for narrow resonances, the latter can be used for both narrow and wide resonant states. While the complex-energy framework has been successfully used to describe radii of halo nuclei [21–24], many questions related to the interpretation of complex expectation values in resonant states remain [25–33].

As stated above, due to their long lifetimes, proton emitters are splendid examples of complex-energy resonant states [34–40]. Broad proton resonances can also be described in terms of the TDSE [41–47]. In this study, we use both methods to investigate and interpret complex rms radii of proton-unbound states.

*Method.* — This study focuses on single-proton emitters, in which the valence proton is coupled to the daughter nucleus (core) [48, 49]. The effective radial nucleon-

\* Email: wangsimin@fudan.edu.cn

† Email: witek@frib.msu.edu

core potential,  $V(r)$ , includes the nuclear interaction in the form of a Woods-Saxon (WS) potential with the spin-orbit term, the Coulomb interaction, and the centrifugal potential. The solutions of the Schrödinger equation with the potential  $V$  that have purely outgoing asymptotic behavior are Gamow/resonant states. The resonant eigenfunction  $\Phi^{J\ell M}(k, \mathbf{r}) = \psi_{J\ell}(k, r)Y_{J\ell M}(\Omega)$  has angular quantum numbers  $(J, \ell, M)$  and corresponds to momentum  $k$  with energy  $E = \hbar^2 k^2 / 2\mu$ . To ensure the outgoing asymptotic behavior, the radial wave function  $u_{J\ell}(k, r) = r\psi_{J\ell}(k, r)$  is expanded in the Berggren basis [50, 51]. The corresponding eigenenergy is complex,  $\tilde{E} = Q_p - i\Gamma/2$ , where  $Q_p$  is the decay energy and  $\Gamma$  is the decay width related to the half-life  $T_{1/2} = \hbar \ln 2 / \Gamma$ .

Unlike in the standard Hilbert-space framework, resonant wave functions belong to the Rigged Hilbert space (RHS) [52, 53]; they are not  $L^2$  square-integrable. In RHS, both bound and resonant states are normalized according to a bi-orthogonal inner product [54]. For resonant states, the radial wave function  $u_{J\ell}(k, r)$  asymptotically approaches the outgoing Coulomb wave function  $H_{\ell, \eta}^+(kr)$ , scaled by an asymptotic normalization coefficient (ANC)  $a_{J\ell}(k)$  where  $\eta$  is the Sommerfeld parameter. Since  $H_{\ell, \eta}^+(kr)$  exhibits oscillatory behavior at large  $r$ , the contribution from the asymptotic region to the normalization integral largely cancels out.

To avoid the divergence of the rms radius of resonant states, a complex radius  $\tilde{r}_{\text{rms}}$  can be introduced, defined as

$$\tilde{r}_{\text{rms}}^2 \equiv \langle \tilde{\psi} | r^2 | \psi \rangle = \int_0^\infty (r\psi)^2 r^2 dr. \quad (1)$$

To evaluate this integral, the exterior complex scaling method is employed [55] by introducing the rotated complex contour  $\mathcal{C}$  corresponding to the complex-scaled radius  $\tilde{r}$ :

$$\tilde{r} = \begin{cases} r, & \text{for } r \leq R_0; \\ R_0 + (r - R_0)e^{i\theta}, & \text{for } r > R_0, \end{cases} \quad (2)$$

where  $R_0$  is the end point at which the complex rotation is applied and  $\theta$  is the rotation angle. Under this transformation, Eq. (1) becomes

$$\tilde{r}_{\text{rms}}^2 = \int_0^{R_0} r^4 \psi^2 dr - \int_{\mathcal{C}} \tilde{r}^2 a_{J\ell}^2 (H_{\ell, \eta}^+)^2 d\tilde{r}. \quad (3)$$

The convergence at large  $|\tilde{r}|$  is ensured by choosing  $\theta > \arctan[\text{Im}(\tilde{k})/\text{Re}(\tilde{k})]$ , so that the factor  $e^{i\tilde{k}\tilde{r}}$  in the asymptotic form of the wave function decays exponentially along  $\mathcal{C}$ .

To relate the complex radius in the resonant state to the measured rms radius, we employ the time-dependent approach [46] to track the evolution of the decaying nucleon. Here, the initial state is modeled by means of the Two Potential Approach (TPA) [56, 57], in which the closed initial potential  $V_{\text{TPA}}(r)$  is assumed to be constant  $V(r_{\text{TPA}}) > Q_p$  for  $r \geq r_{\text{TPA}}$  (see Fig. S1 in Supplemental

Material (SM) [58] for illustration), where  $r_{\text{TPA}}$  is chosen inside the barrier (between the barrier radius and outer turning point) [57]. As shown below, the evolution during the moderate time period is governed by the resonant dynamics of the state and is essentially insensitive to the choice of  $r_{\text{TPA}}$ .

Our analysis is carried out for the rms radius of  $d_{5/2}$  resonant state in the proton emitter  $^{15}\text{F}(^{14}\text{O}+p)$ , a medium-mass nucleus with moderate decay width [59, 60], which constitutes excellent laboratory for various open quantum system phenomena [45, 60–62].

*Hamiltonian and parameters.* — Unless stated otherwise, the exterior complex scaling is carried out with  $R_0 = 20$  fm and the rotation angle  $\theta = \pi/4$ . The depth of the WS potential,  $V_0$ , is varied to control the resonance energy; all remaining parameters follow the ‘universal’ WS parameterization [63]. The Berggren basis employs the complex-momentum contour  $k = 0 \rightarrow 0.3 - 0.2i \rightarrow 0.5 - 0.15i \rightarrow 0.6 \rightarrow 0.8 \rightarrow 1.2 \rightarrow 2 \rightarrow 4 \rightarrow 6$  (all in  $\text{fm}^{-1}$ ). Each segment is discretized with 80 points. For real-time propagation, we project the contour onto the real axis, thereby restoring the Hamiltonian’s Hermiticity and ensuring norm (density) conservation. In practice, the initial wave function within a sphere of radius  $R_{\text{cut}} = 50$  fm is expanded in real-momentum space. Noticing this procedure does not impact the asymptotic boundary condition, the results remain unaffected as long as  $R_{\text{cut}}$  exceeds the spatial extent of the localized initial wave function and the analysis region used for evaluating the radius and other observables (see videos in the Supplemental Material [58]). The parameter  $r_{\text{TPA}}$  is chosen to match the radii obtained from the complex-scaling and time-dependent analyses.

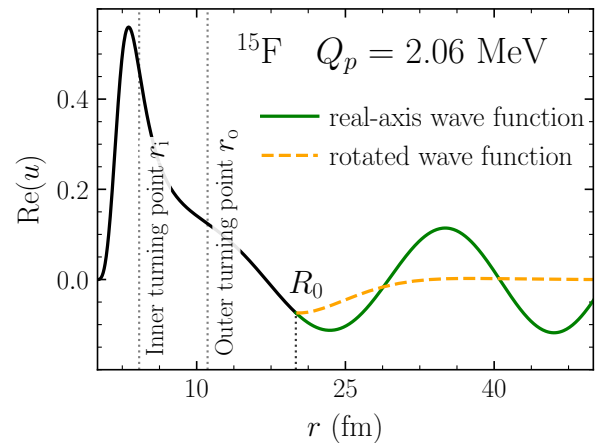


FIG. 1. Real part of the  $d_{5/2}$  radial wave function  $u$  in  $^{15}\text{F}$  at  $Q_p = 2.06$  MeV evaluated along the real axis  $r$  (solid line) and along the complex-rotated coordinate  $\tilde{r}$  (dashed line), see Eq. (2). The inner ( $r_i$ ) and outer ( $r_o$ ) turning points are indicated by dotted lines.

*Complex radius.* — Figure 1 shows the wave function of the resonant state in  $^{15}\text{F}$  at  $Q_p = 2.06$  MeV along the real- $r$  axis and along the rotated contour  $\mathcal{C}$ . The wave

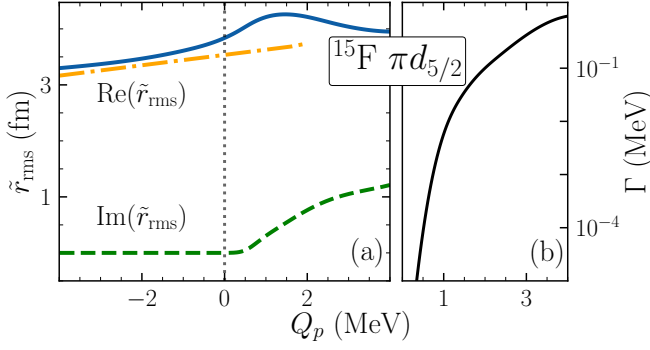


FIG. 2. (a) Complex-rms radius  $\tilde{r}_{\text{rms}}$  and (b) decay width  $\Gamma$  as a function of decay energy  $Q_p$  calculated for the proton resonant  $d_{5/2}$  state in  $^{15}\text{F}$ . The real and imaginary parts of  $\tilde{r}_{\text{rms}}$  are shown by the solid and dashed lines, respectively. The dash-dotted line shows the rms radius in the HO basis, i.e., without continuum coupling. The proton threshold is marked by the dotted line.

function is localized in the nuclear interior, and it decays exponentially inside the barrier. Outside the outer turning point  $r_o$ , the resonant wave function  $u(r)$  exhibits oscillatory behavior. The rotation radius  $R_0$  defining the contour  $\mathcal{C}$  is chosen beyond  $r = r_o$ . With this choice, the rotated wave function  $u(\tilde{r})$  quickly decays to zero. As shown in Table S1 of SM [58], the computed complex rms radii are practically independent of the choice of  $\mathcal{C}$ .

For bound states, the complex radius  $\tilde{r}_{\text{rms}}$  reduces to the usual rms radius  $r_{\text{rms}}$ . Once the state crosses the decay threshold, it becomes a resonance characterized by a complex energy  $\tilde{E}$ , where the real part  $Q_p$  corresponds to the average value of energy and the imaginary part  $\Gamma$  is related to the energy uncertainty [25, 50]. The same interpretation applies to any complex quantity commuting with the Hamiltonian [25, 50], and can be extended to self-adjoint operators—such as the radius operator—within the framework of tempered ultradistributions and Gel'fand triplets by considering the leading-order terms in  $\Gamma$  [27, 28, 30].

As shown in Fig. 2(a), the imaginary part of the complex radius increases with the decay energy, correlating strongly with the growth of the decay width [64] in Fig. 2(b). In contrast, the real part exhibits a non-monotonic trend: it initially increases as the wave function becomes more diffuse in the asymptotic region during evolution from a bound to a resonant state, but beyond a certain point it decreases with increasing decay energy. As discussed below, this behavior reflects the interplay between the spatial extension and the finite lifetime of the resonant wave function.

To extract the continuum-coupling contribution to the rms radius, we carry out calculations in the harmonic oscillator (HO) basis by considering the lowest four radial node  $d_{5/2}$  states. The difference between the Berggren-basis calculations and HO results shown in Fig. 2(a) gradually increases from  $Q_p \approx -1$  MeV and becomes quite appreciable above the proton threshold. This is a mani-

festation of a proton halo effect.

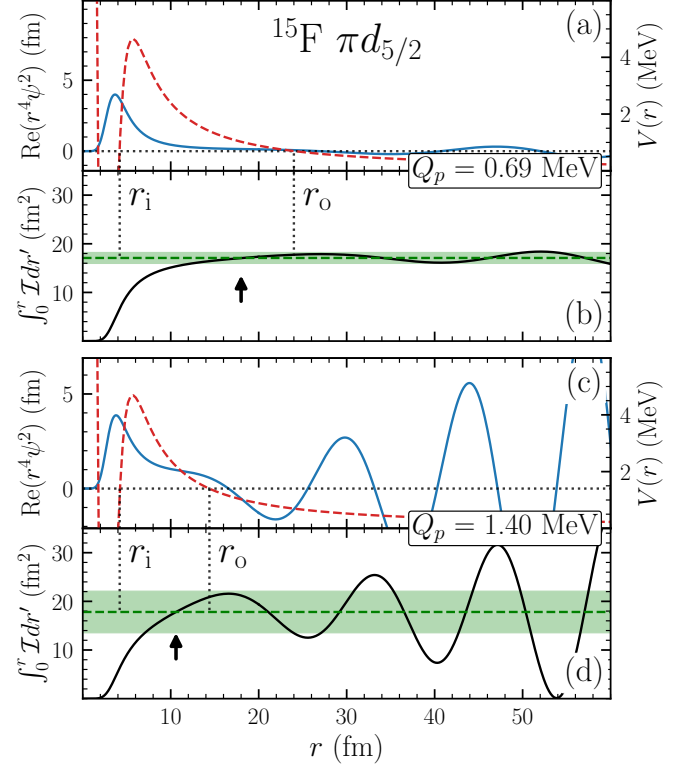


FIG. 3. Complex radius integrand  $r^4\psi^2$  (a, c) and the corresponding cumulative integral  $\int_0^r r'^4\psi^2 dr'$  (b, d) for the proton resonant  $d_{5/2}$  state in  $^{15}\text{F}$  at  $Q_p = 0.69$  MeV (top) and 1.40 MeV (bottom). All quantities are evaluated along the real axis without complex rotation. The dashed line indicates the potential barrier. The dash-dotted line and shaded bar mark the real and imaginary part of the complex radius  $\tilde{r}_{\text{rms}}$ , respectively. The inner and outer turning points are indicated. The intersection point at which the cumulative integral becomes equal to the complex rms radius is shown by an arrow.

To understand this non-monotonic behavior of  $\Re(\tilde{r}_{\text{rms}})$  seen in Fig. 2(a), in Fig. 3 we examine the integrand  $r^4\psi^2$  defining the complex rms radius, along with the cumulative integral  $\int_0^r r'^4\psi^2 dr'$ , both plotted along the real coordinate  $r$ . The wave function of the resonant state exhibits oscillatory behavior with increasing amplitude, as expected for a Gamow state [65]. Since the contribution to the rms radius from the asymptotic region is largely canceled out, it is the internal part of the wave function that determines the complex radius.

Importantly, the point at which the cumulative integral of  $r^4\psi^2$  intersects the complex radius  $\tilde{r}_{\text{rms}}^2$  appears close to the outer turning point. As the decay energy increases, the effective barrier becomes lower and narrower, leading to a reduction of the barrier-penetration region. Concurrently, the interior part of the wave function is reduced. At sufficiently high energies, the decrease of the wave function in the inner and barrier regions results in a slight decrease of the rms radius.

*Time dependent analysis.* — The concept of complex observables has been broadly employed across atomic, hadronic, and nuclear physics [24, 25, 27, 30–33]. Yet, a direct demonstration linking these complex quantities to measurable observables remains lacking. In reality, a resonant state decays within a finite lifetime, during which its spatial distribution evolves from an initially localized wave packet into outgoing decay fragments, accompanied by a change in its radius. We quantify this process by computing the time-dependent rms radius for various decay energies and comparing it with the complex rms radius. The initial time  $t = 0$  is defined as the moment immediately following the formation, when the decaying proton is confined within the parent nucleus. This wave function is subsequently propagated with the Hermitian Hamiltonian in the standard Hilbert space.

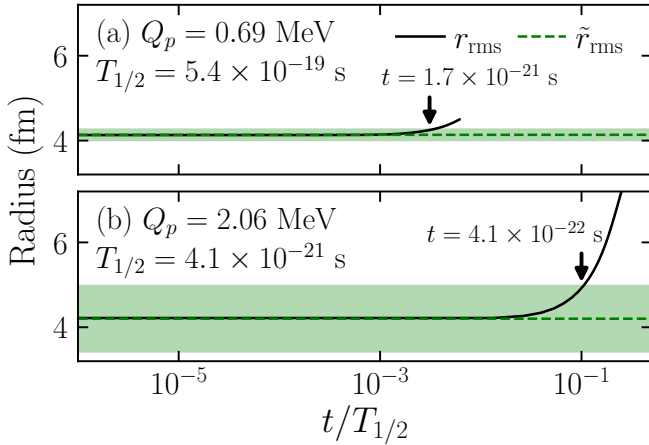


FIG. 4. Time evolution of the rms radius  $r_{\text{rms}}$  of the  $d_{5/2}$  resonance in  $^{15}\text{F}$  (solid line) as a function of time  $t$  (in units of the half-life  $T_{1/2}$ ) for (a)  $Q_p = 0.69$  MeV and (b)  $Q_p = 2.06$  MeV. The real (dashed line) and imaginary (shaded band) parts of the complex radius  $\tilde{r}_{\text{rms}}$  are shown for comparison. The uncertainty in  $r_{\text{rms}}$  related to the variation of  $r_{\text{TPA}}$  by  $\pm 1$  fm is marked by a gray band. Arrows mark the time at which  $r_{\text{rms}}$  start departing from  $\Re(\tilde{r}_{\text{rms}})$  within the uncertainty  $\Im(\tilde{r}_{\text{rms}})$ .

During the time evolution, the valence nucleon is emitted and the system’s wave function becomes progressively more diffuse (see Figs. S2 and S3 in SM [58]), leading to an eventual increase of  $r_{\text{rms}}$ . As shown in Fig. 4, the rate of increase correlates with the width  $\Gamma$  (or half-life  $T_{1/2}$ ). The calculated time evolution exhibits clean exponential decay for all investigated energies over a broad temporal window, confirming the numerical accuracy of the propagation (See Fig. S6 in SM [58]). Caution is nevertheless required when evaluating the radius: since the wave function is represented in the momentum space (Berggren basis) while  $r_{\text{rms}}$  is computed in coordinate space, numerical stability demands that the asymptotic tail be well converged and contained within the analysis box. Any leakage or incomplete convergence may distort the later-time behavior, particularly for long-lived states. To control this effect, the evolution is restricted to the early

times when the total leakage remains below 0.01%. This limitation, however, does not affect the survival probability  $|\langle\Phi(t)|\Phi(0)\rangle|^2$  (see Fig. S6 in SM [58]), where the localized initial state naturally suppresses contributions from the escaped flux.

Theoretically, the squared rms radius  $r_{\text{rms}}^2$  follows an approximately quadratic behavior at the early stage of the decay process,

$$r_{\text{rms}}^2(t) \simeq r_{\text{rms}}^2(0) + b_{\text{TPA}} t^2, \quad (4)$$

where  $b_{\text{TPA}} = \langle \mathbf{r} \cdot \nabla (V_{\text{TPA}} - V) / m \rangle_{t=0}$  (see SM [58] for the derivation). Since  $V_{\text{TPA}}$  and  $V$  differ only in the asymptotic region — where the quasi-bound initial wave function is negligible and the potential varies smoothly —  $b_{\text{TPA}}$  is small in magnitude. Consequently, at early times,  $t \lesssim 10^{-3} T_{1/2}$ , the standard rms radius remains essentially constant and coincides with the complex rms radius. This early-time plateau reflects the generic short-time, non-exponential regime in which the decay rate vanishes at  $t = 0$  [66–70], and connects to state preparation and the quantum Zeno effect, wherein frequent measurement can inhibit decay [71–74]. This indicates that a radius measurement performed on timescales short compared to  $T_{1/2}$  — feasible for sufficiently long-lived systems — should be consistent with the complex rms radius of the Gamow state. At later times, the squared rms radius  $r_{\text{rms}}^2$  increases slowly and approximately quadratically with time. The growth rate  $b_{\text{TPA}}$  depends weakly on the matching radius  $r_{\text{TPA}}$  adopted in the TPA approach (see Fig. S4 in SM [58]), reflecting the residual sensitivity to the quantum state-preparation process. And the calculated radius evolution is in a close agreement with the expression (4).

To test the robustness of the extracted radius against the choice of initial conditions, we vary  $r_{\text{TPA}}$  within  $\pm 1$  fm. The resulting spread of  $r_{\text{rms}}$  (narrow gray band in Fig. 4) is negligible and does not affect the overall trend. Indeed, at intermediate times, the nonresonant scattering components of the initial state quickly disperse, leaving the evolution predominantly governed by the resonant contribution [46, 47]. Moreover, we also examined the full physically relevant range of  $r_{\text{TPA}}$ , from the barrier top to the outer turning point  $r_o$  (6 – 23 fm for the  $Q_p = 0.69$  MeV state; see Fig. 3). The initial  $r_{\text{rms}}$  increases gradually with  $r_{\text{TPA}}$  (see Fig. S5 in SM [58]), yet the resulting values remain largely within the uncertainty  $\Im(\tilde{r}_{\text{rms}})$ , with the central value corresponding to  $\Re(\tilde{r}_{\text{rms}})$ . This indicates that the complex radius  $\tilde{r}_{\text{rms}}$  effectively represents the mean spatial configuration of the states formed within the barrier. Interestingly, the value of  $r_{\text{TPA}}$  at which  $r_{\text{rms}}$  equals  $\Re(\tilde{r}_{\text{rms}})$  approximately coincides with the minimum of the  $r_{\text{rms}}$  growth rate as a function of  $r_{\text{TPA}}$ .

*Summary.* — A complex rms radius of the resonant state is evaluated for the  $d_{5/2}$  state of proton emitter  $^{15}\text{F}$  using the exterior complex scaling. This quantity remains finite for unbound states, with its imaginary



part being interpreted as an uncertainty associated with the decay width. The complex radius exhibits a non-monotonic evolution across the decay threshold that is governed by the competition between an outward shift of the density and the barrier-driven depletion of the interior. In particular, we predict a proton halo effect in proton emitters that manifests itself in a local increase of the charge radius around the decay threshold.

A complementary real-time analysis further demonstrates that, during the early stage of decay, the standard rms radius remains essentially constant and coincides with the complex rms radius, providing an operational route for charge radii measurements in proton emitters. Although  $^{15}\text{F}$  itself is too short-lived for direct measurement, its radius evolution exhibits universal features expected to be present in longer-lived systems. Our theoretical framework is robust against variations of complex-scaling parameters and initial preparation, and it is readily extendable to other complex observables in open quantum systems.

*Acknowledgments.* — This material is based upon work supported by the National Key Research and Development Program (MOST 2023YFA1606404 and MOST 2022YFA1602303); the National Natural Science Foundation of China under Contract No. 12347106 and No. 12147101; and by the U.S. Department of Energy under Award Number DE-SC0013365 (Office of Science, Office of Nuclear Physics) and DE-SC0023175 (Office of Science, NUCLEI SciDAC-5 collaboration).

*Data availability.* — The data are not publicly available. The data are available from the authors upon reasonable request.

- 
- [1] M. Thoennessen, Reaching the limits of nuclear stability, *Rep. Prog. Phys.* **67**, 1187 (2004).
  - [2] W. Nazarewicz and L. Sobotka, The lessons learned from ephemeral nuclei, *Phys. Today* **78**, 30 (2025).
  - [3] V. I. Goldansky, On neutron-deficient isotopes of light nuclei and the phenomena of proton and two-proton radioactivity, *Nucl. Phys.* **19**, 482–495 (1960).
  - [4] B. Blank and M. J. G. Borge, Nuclear structure at the proton drip line: Advances with nuclear decay studies, *Prog. Part. Nucl. Phys.* **60**, 403–483 (2008).
  - [5] B. Blank and R. D. Page, Charged-Particle Radioactive Decays, in *Handbook of Nuclear Physics*, edited by I. Tanihata, H. Toki, and T. Kajino (Springer Nature Singapore, Singapore, 2023) pp. 399–442.
  - [6] M. Pfützner, M. Karny, L. V. Grigorenko, and K. Riisager, Radioactive decays at limits of nuclear stability, *Rev. Mod. Phys.* **84**, 567–619 (2012).
  - [7] M. Pfützner, I. Mukha, and S. M. Wang, Two-proton emission and related phenomena, *Prog. Part. Nucl. Phys.* **132**, 104050 (2023).
  - [8] M. Pfützner and C. Mazzocchi, Nuclei Near and at the Proton Dripline, in *Handbook of Nuclear Physics*, edited by I. Tanihata, H. Toki, and T. Kajino (Springer Nature Singapore, Singapore, 2023) pp. 1295–1335.
  - [9] E. Olsen, M. Pfützner, N. Birge, M. Brown, W. Nazarewicz, and A. Perhac, Landscape of Two-Proton Radioactivity, *Phys. Rev. Lett.* **110**, 222501 (2013).
  - [10] L. Neufcourt, Y. Cao, S. Giuliani, W. Nazarewicz, E. Olsen, and O. B. Tarasov, Beyond the proton drip line: Bayesian analysis of proton-emitting nuclei, *Phys. Rev. C* **101**, 014319 (2020).
  - [11] R. Kanungo, Radii and Momentum Distribution of Unstable Nuclei, in *Handbook of Nuclear Physics*, edited by I. Tanihata, H. Toki, and T. Kajino (Springer Nature Singapore, Singapore, 2023) pp. 1081–1124.
  - [12] G. D. Alkhazov, I. S. Novikov, and Y. M. Shabelski, Nuclear radii of unstable nuclei, *Int. J. Mod. Phys. E* **20**, 583–627 (2011).
  - [13] E. W. Otten, Nuclear Radii and Moments of Unstable Isotopes, in *Treatise on Heavy Ion Science: Volume 8: Nuclei Far From Stability*, edited by D. A. Bromley (Springer US, Boston, MA, 1989) pp. 517–638.
  - [14] W. Nörtershäuser and I. D. Moore, Nuclear Charge Radii, in *Handbook of Nuclear Physics*, edited by I. Tanihata, H. Toki, and T. Kajino (Springer Nature Singapore, Singapore, 2023) pp. 243–312.
  - [15] B. Cheal *et al.*, *Laser spectroscopy of neutron-deficient thulium isotopes* (2022).
  - [16] K. Lynch *et al.*, *In-source laser spectroscopy of neutron-deficient lutetium and holmium isotopes, towards the proton emitters* (2024).
  - [17] A. S. Jensen, K. Riisager, D. V. Fedorov, and E. Garrido, Structure and reactions of quantum halos, *Rev. Mod. Phys.* **76**, 215–261 (2004).
  - [18] A. J. Miller *et al.*, Proton superfluidity and charge radii in proton-rich calcium isotopes, *Nat. Phys.* **15**, 432–436 (2019).
  - [19] P.-G. Reinhard and W. Nazarewicz, Information content of the differences in the charge radii of mirror nuclei, *Phys. Rev. C* **105**, L021301 (2022).
  - [20] Z. C. Xu, S. M. Wang, T. Beck, A. Gade, and W. Nazarewicz, Puzzling  $B(E2; 0^+ \rightarrow 2^+)$  strength in the proton dripline nucleus  $^{36}\text{Ca}$ , *Phys. Rev. C* **112**, L011302 (2025).
  - [21] T. Myo, R. Ando, and K. Katō, Five-body resonances of  $^8\text{He}$  using the complex scaling method, *Phys. Lett. B* **691**, 150–155 (2010).
  - [22] G. Papadimitriou, A. T. Kruppa, N. Michel, W. Nazarewicz, M. Płoszajczak, and J. Rotureau, Charge radii and neutron correlations in helium halo nuclei, *Phys. Rev. C* **84**, 051304 (2011).
  - [23] A. T. Kruppa, G. Papadimitriou, W. Nazarewicz, and N. Michel, Nuclear three-body problem in the complex energy plane: Complex-Scaling-Slater method, *Phys. Rev. C* **89**, 014330 (2014).
  - [24] T. Myo and K. Katō, Mirror symmetry breaking in He isotopes and their mirror nuclei, *Prog. Theor. Exp. Phys.* **2014**, 083D01 (2014).
  - [25] T. Berggren, Expectation value of an operator in a resonant state, *Phys. Lett. B* **373**, 1–4 (1996).
  - [26] A. Bührers and J.-M. Rost, Complex expectation values and lewis structures for resonant states, *J. Phys. B* **29**, 3825 (1996).
  - [27] C. G. Bollini, O. Civitarese, A. L. De Paoli, and M. C. Rocca, Physical representations of Gamow states in a rigged Hilbert space, *Phys. Lett. B* **382**, 205–208 (1996).
  - [28] C. G. Bollini, O. Civitarese, A. L. De Paoli, and M. C. Rocca, Gamow states as continuous linear functionals

- over analytical test functions, *J. Math. Phys.* **37**, 4235–4242 (1996).
- [29] M. Homma, T. Myo, and K. Katō, Matrix Elements of Physical Quantities Associated with Resonance States, *Prog. Theor. Phys.* **97**, 561–567 (1997).
- [30] O. Civitarese, M. Gadella, and R. I. Betan, On the mean value of the energy for resonant states, *Nucl. Phys. A* **660**, 255–266 (1999).
- [31] T. Sekihara and T. Hyodo, Size measurement of dynamically generated hadronic resonances with finite boxes, *Phys. Rev. C* **87**, 045202 (2013).
- [32] G. Papadimitriou, Calculation of Expectation Values of Operators in the Complex Scaling Method, *Few-Body Syst.* **57**, 833–849 (2016).
- [33] T. Myo and K. Katō, Possible interpretation of the complex expectation values associated with resonances, *Phys. Rev. C* **107**, 014301 (2023).
- [34] L. S. Ferreira, E. Maglione, and R. J. Liotta, Nucleon Resonances in Deformed Nuclei, *Phys. Rev. Lett.* **78**, 1640–1643 (1997).
- [35] E. Maglione, L. S. Ferreira, and R. J. Liotta, Proton emission from deformed nuclei, *Phys. Rev. C* **59**, R589–R592 (1999).
- [36] K. Rykaczewski *et al.*, Proton emitters  $^{140}\text{Ho}$  and  $^{141}\text{Ho}$ : Probing the structure of unbound Nilsson orbitals, *Phys. Rev. C* **60**, 011301 (1999).
- [37] A. T. Kruppa, B. Barmore, W. Nazarewicz, and T. Vertse, Fine Structure in the Decay of Deformed Proton Emitters: Nonadiabatic Approach, *Phys. Rev. Lett.* **84**, 4549–4552 (2000).
- [38] B. Barmore, A. T. Kruppa, W. Nazarewicz, and T. Vertse, Theoretical description of deformed proton emitters: Nonadiabatic coupled-channel method, *Phys. Rev. C* **62**, 054315 (2000).
- [39] S. M. Wang, N. Michel, W. Nazarewicz, and F. R. Xu, Structure and decays of nuclear three-body systems: The Gamow coupled-channel method in Jacobi coordinates, *Phys. Rev. C* **96**, 044307 (2017).
- [40] S. M. Wang and W. Nazarewicz, Puzzling Two-Proton Decay of  $^{67}\text{Kr}$ , *Phys. Rev. Lett.* **120**, 212502 (2018).
- [41] P. Talou, N. Carjan, and D. Strottman, Time-dependent properties of proton decay from crossing single-particle metastable states in deformed nuclei, *Phys. Rev. C* **58**, 3280–3285 (1998).
- [42] P. Talou, N. Carjan, and D. Strottman, Time-dependent approach to bidimensional quantum tunneling: application to the proton emission from deformed nuclei, *Nucl. Phys. A* **647**, 21–46 (1999).
- [43] T. Oishi, K. Hagino, and H. Sagawa, Role of diproton correlation in two-proton-emission decay of the  $^6\text{Be}$  nucleus, *Phys. Rev. C* **90**, 034303 (2014).
- [44] T. Oishi, Time-dependent Dirac equation applied to one-proton radioactive emission, *Phys. Rev. C* **107**, 034301 (2023).
- [45] T. Oishi and M. Kimura, Interference of resonances in two-proton emission of  $^{16}\text{Ne}$ , *Phys. Rev. C* **111**, 044319 (2025).
- [46] S. M. Wang and W. Nazarewicz, Fermion Pair Dynamics in Open Quantum Systems, *Phys. Rev. Lett.* **126**, 142501 (2021).
- [47] S. M. Wang, W. Nazarewicz, A. Volya, and Y. G. Ma, Probing the nonexponential decay regime in open quantum systems, *Phys. Rev. Res.* **5**, 023183 (2023).
- [48] B. Buck, A. C. Merchant, and S. M. Perez, Ground state proton emission from heavy nuclei, *Phys. Rev. C* **45**, 1688–1692 (1992).
- [49] S. Åberg, P. B. Semmes, and W. Nazarewicz, Spherical proton emitters, *Phys. Rev. C* **56**, 1762–1773 (1997).
- [50] T. Berggren, On the use of resonant states in eigenfunction expansions of scattering and reaction amplitudes, *Nucl. Phys. A* **109**, 265–287 (1968).
- [51] N. Michel, W. Nazarewicz, M. Płoszajczak, and T. Vertse, Shell model in the complex energy plane, *J. Phys. G* **36**, 013101 (2009).
- [52] J.-P. Antoine, R. Bishop, A. Bohm, and S. Wickramasekara, Rigged Hilbert spaces in quantum physics, in *Compendium of Quantum Physics*, edited by D. Greenberger, K. Hentschel, and F. Weinert (Springer, Berlin, Heidelberg, 2009) pp. 640–650.
- [53] N. Michel and M. Płoszajczak, *Gamow Shell Model: The Unified Theory of Nuclear Structure and Reactions*, Lecture Notes in Physics, Vol. 983 (Springer, Cham, 2021).
- [54] N. Moiseyev, P. R. Certain, and F. Weinhold, Resonance properties of complex-rotated hamiltonians, *Mol. Phys.* **36**, 1613–1630 (1978).
- [55] B. Gyarmati and T. Vertse, On the normalization of Gamow functions, *Nucl. Phys. A* **160**, 523–528 (1971).
- [56] S. A. Gurvitz and G. Kalbermann, Decay width and the shift of a quasistationary state, *Phys. Rev. Lett.* **59**, 262–265 (1987).
- [57] S. A. Gurvitz, P. B. Semmes, W. Nazarewicz, and T. Vertse, Modified two-potential approach to tunneling problems, *Phys. Rev. A* **69**, 042705 (2004).
- [58] See Supplemental Material at [URL inserted by publisher] for details on the time-dependent rms radius, supplementary table and figures of its properties, and videos illustrating the time dynamics.
- [59] I. Mukha *et al.*, Spectroscopy of proton-unbound nuclei by tracking their decay products in-flight: One- and two-proton decays of  $^{15}\text{F}$ ,  $^{16}\text{Ne}$ , and  $^{19}\text{Na}$ , *Phys. Rev. C* **82**, 054315 (2010).
- [60] V. Girard-Alcindor *et al.*, New narrow resonances observed in the unbound nucleus  $^{15}\text{F}$ , *Phys. Rev. C* **105**, L051301 (2022).
- [61] J. Okołowicz and M. Płoszajczak, Exceptional points in the scattering continuum, *Phys. Rev. C* **80**, 034619 (2009).
- [62] J. Okołowicz and M. Płoszajczak, Near-threshold configuration mixing, *Acta Phys. Pol. B* **42**, 451 (2011).
- [63] J. Dudek, Z. Szymański, and T. Werner, Woods-Saxon potential parameters optimized to the high spin spectra in the lead region, *Phys. Rev. C* **23**, 920–925 (1981).
- [64] B. Gyarmati, F. Krisztinkovics, and T. Vertse, On the expectation value in Gamow state, *Phys. Lett. B* **41**, 110–112 (1972).
- [65] A. I. Baz', Y. B. Zel'dovich, and A. M. Perelomov, *Scattering, reactions and decay in nonrelativistic quantum mechanics* (Israel Program for Scientific Translation, Jerusalem, 1969).
- [66] L. Fonda, G. C. Ghirardi, and A. Rimini, Decay theory of unstable quantum systems, *Rep. Prog. Phys.* **41**, 587–631 (1978).
- [67] J. M. Deutsch, Eigenstate thermalization hypothesis, *Rep. Prog. Phys.* **81**, 082001 (2018).
- [68] T. Gorin, T. Prosen, T. H. Seligman, and M. Žnidarič, Dynamics of Loschmidt echoes and fidelity decay, *Phys. Rep.* **435**, 33–156 (2006).
- [69] A. Volya and V. Zelevinsky, Time-dependent relaxation of observables in complex quantum systems, *J. Phys. Complex.* **1**, 025007 (2020).

- [70] M. Peshkin, A. Volya, and V. Zelevinsky, Non-exponential and oscillatory decays in quantum mechanics, [Europhys. Lett. \*\*107\*\*, 40001 \(2014\)](#).
- [71] G. C. Ghirardi, C. Omero, T. Weber, and A. Rimini, Small-time behaviour of quantum nondecay probability and Zeno's paradox in quantum mechanics, [Nuov. Cim. A \*\*52\*\*, 421–442 \(1979\)](#).
- [72] C. B. Chiu, E. C. G. Sudarshan, and B. Misra, Time evolution of unstable quantum states and a resolution of Zeno's paradox, [Phys. Rev. D \*\*16\*\*, 520–529 \(1977\)](#).
- [73] A. G. Kofman and G. Kurizki, Quantum Zeno effect on atomic excitation decay in resonators, [Phys. Rev. A \*\*54\*\*, R3750–R3753 \(1996\)](#).
- [74] S. R. Wilkinson, C. F. Bharucha, M. C. Fischer, K. W. Madison, P. R. Morrow, Q. Niu, B. Sundaram, and M. G. Raizen, Experimental evidence for non-exponential decay in quantum tunnelling, [Nature \*\*387\*\*, 575–577 \(1997\)](#).